Combined cosmological tests of a bivalent tachyonic dark energy scalar field model

Zoltán Keresztes and László Á. Gergely

Departments of Theoretical and Experimental Physics, University of Szeged, Dóm tér 9, 6720 Szeged, Hungary

E-mail: zkeresztes@titan.physx.u-szeged.hu,gergely@physx.u-szeged.hu

Abstract. A recently investigated tachyonic scalar field dark energy dominated universe exhibits a bivalent future: depending on initial parameters can run either into a de Sitter exponential expansion or into a traversable future soft singularity followed by a contraction phase. We also include in the model (i) a tiny amount of radiation, (ii) baryonic matter ($\Omega_b h^2 = 0.022161$, where the Hubble constant is fixed as $h = 0.706$) and (iii) cold dark matter (CDM). Out of a variety of six types of evolutions arising in a more subtle classification, we identify two in which in the past the scalar field effectively degenerates into a dust (its pressure drops to an insignificantly low negative value). These are the evolutions of type IIb converging to de Sitter and type III hitting the future soft singularity. We confront these background evolutions with various cosmological tests, including the supernova type Ia Union 2.1 data, baryon acoustic oscillation distance ratios, Hubble parameter-redshift relation and the cosmic microwave background (CMB) acoustic scale. We determine a subset of the evolutions of both types which at 1σ confidence level are consistent with all of these cosmological tests. At perturbative level we derive the CMB temperature power spectrum to find the best agreement with the Planck data for $\Omega_{CDM} = 0.22$. The fit is as good as for the ΛCDM model at high multipoles, but the power remains slightly overestimated at low multipoles, for both types of evolutions. The rest of the CDM is effectively generated by the tachyonic field, which in this sense acts as a combined dark energy and dark matter model.

Contents

1 Introduction

The discovery of the accelerated expansion rate of the Universe at late times [1] induced the necessity to model dark energy, the unknown energy form responsible for such a phenomenon. Beyond the simple, but conceptually unsatisfactory cosmological constant wide classes of dark energy models were investigated. The most common models introduce a scalar field ϕ as dark energy candidate. In the simplest, quintessence models [2] the dynamics of the scalar field is encompassed in the Lagrangian density $\mathcal{L} = \sqrt{-g}L$ through the canonical Lagrangian $L = X - \mathcal{V}(\phi)$ (here g, X, $\mathcal{V}$ stand for the metric determinant, standard kinetic term X and potential term $\mathcal{V}$). Generalized k-essence models [3] exhibit a Lagrangian with non-standard dependence of the kinetic term, hence $L = P(\phi, X)$, with P an arbitrary function. A particular subcase of the latter is obtained when $L = -V(\phi)\sqrt{1-2X}$, thus it has the Dirac-Born-Infeld form [4]. In this latter case the scalar $\phi \equiv T$ is known as a tachyonic field.

If the scalar field depends solely on time (which is the case in the presence of cosmological symmetries), its energy-momentum tensor characterizes a perfect fluid. In particular, a time-dependent, homogeneous tachyonic field can be perceived as a perfect fluid. (When the potential V is a constant, this fluid becomes the Chaplygin gas, which together with its generalizations was also studied as a dark energy candidate [5].)

It was shown that tachyonic fields with inverse square law or exponential potentials could play the role of dark energy, as they were found consistent with type Ia Supernovae (SNIa) data and with the requirements of structure formation [6]. Furthermore the luminosity-redshift relation arising from SNIa data, the baryon acoustic oscillation (BAO) distance ratios from recent galaxy surveys (BAO are the imprint in the distribution of matter of the sound horizon at the last scattering surface), the Hubble constant measurement from Hubble Space Telescope data and the cosmic microwave background (CMB) temperature anisotropy

can be explained by a scalar field (quintessence or tachyonic) dark energy with equation of state $p = c_a^2 \rho + C$ with constants c_a^2 and C [7].

The dynamics of tachyonic cosmological models can be quite rich, depending on the chosen potential. For the trigonometric potential discussed in Ref. [8] some of the future evolutions, rather then asymptoting to the de Sitter attractor, will exhibit a slowdown of the accelerated expansion (during which the tachyonic field still behaves as dark energy), then continue through a decelerated regime (when the tachyonic field ceases to mimic dark energy and it evolves superluminally) until the deceleration reaches infinite value and the expansion suddenly stops. This is a specific example of a future sudden singularity [9] dubbed Big Brake [8], characterized by finite values of the scale factor, vanishing energy density and Hubble parameter, but diverging deceleration and infinite pressure.

The question naturally arises whether such evolutions can actually be realized in our Universe. In Ref. [10] the observational data on SNIa was confronted with the evolutions of the universe filled with such a one-parameter family of tachyonic models. Among the set of the trajectories of the model compatible with the SNIa data at 1σ level, a subset was found to evolve into a Big Brake. The time scales for reaching this singularity are finite, at the order of the present age of the universe.

As shown in Ref. [11] the infinities appearing at the Big Brake only affect the geodesic deviation equation, in the form of infinite tidal forces. The geodesics themselves remain regular, hence they can be continued through the singularity. Once matter particles have passed through, they will determine the new geometry, which turned out to be a recollapsing one, eventually reaching a Big Crunch.

The SNIa test works well also when baryonic and cold dark matter (CDM) are added to the system [12]. The combination of the tachyonic scalar field and dust however leads to an additional problem when reaching the singularity. Despite the tachyonic energy density vanishing at the singularity, the dust still arrives with a nonzero energy density there, hence the expansion rate is nonvanishing. Similar features emerge when adding a dust component to an anti-Chaplygin gas. In both cases the Hubble parameter acquires a nonzero value at the singularity due to the dust component, implying further expansion. With continued expansion however, both the energy density and the pressure would become ill-defined, hence only a contraction would be allowed. The paradox is resolved by suitably redefining the anti-Chaplygin gas in a distributional sense [13]. Then due to a sudden reversal of the expansion rate (a jump in the Hubble parameter) a contraction could instantly follow the expansion phase. This is analogous to a ball bouncing back in a perfectly elastic manner from a wall.

As an alternative, certain transformations of the properties of both the anti-Chaplygin gas and the tachyonic scalar field could lead to a smooth passage through the soft singularity even in the presence of a dust component. The expansion is continued for a while after the singularity, with a full stop arising later on, followed by a contraction, a second passage through the singularity and then further contraction until the Big Crunch is reached [12]. By analogy this process is similar to modeling the deformations of the ball during the collision process with the wall, which will lead to a full stop of the ball at the detriment of its temporary deformation.

A distinct question is how the tachyonic scalar field model evolved in the past. A purely theoretical study [8] indicated that there are five types of cosmological evolutions, all emerging from a Big Bang type singularity (see Fig. 1). Along type III trajectories the tachyonic field exhibits negative pressure in the first era of the evolutions (including a region of the velocity phase diagram where it can mimic dark energy), however the pressure becomes positive later

on and the field evolves into a Big Brake singularity. By contrast, in the evolutions of type V the tachyonic field exhibits positive pressure all the time (hence it doesn't have a dark energy regime, proving itself incompatible with the present day acceleration) and evolves into a Big Brake. In the evolutions of type I and IV both regimes are present: these evolutions all start with a positive pressure regime (hence superluminal evolution of the tachyonic field), then the pressure turns negative (and the tachyonic field evolves subluminally) so that in principle they can mimic dark energy. The evolution of type I goes into the de Sitter attractor, while the evolution IV allows for another change of the sign of the pressure and finally run into a Big Brake. The type II trajectories arise from the Big Bang at $s^2 = 1$ and end in the de Sitter attractor.

In this work we focus on the past evolutions, by confronting them with a powerful set of cosmological observations. Our aim is to find the evolutions which could be realized in our Universe.

In section 2 we briefly present the tachyonic scalar field model with trigonometric potential (for simplicity we do not include other matter types in this section) and revisit the compatibility with the SNIa observations based on the most recent available Union 2.1 data set [14]. We prove here for the first time that only the evolutions of type I, II and III are compatible with SNIa data at 1σ confidence level, disruling those of type IV, which on purely theoretical grounds were also allowed. A further analysis based on test with SNIa and Hubble parameter data [15], [16] shows that only the types II and III are allowed at 1σ confidence level. Next we prove that the evolution of the effective equation of state parameter disrules the trajectories of type I and a subclass of type II evolutions denoted IIa, as they built up significant pressure in the distant past. They also fail to obey basic stability requirements, as the square of the speed of sound becomes negative. The rest of the trajectories of type II denoted IIb and all of type III survive these tests. The division of the trajectories of type II into IIa and IIb enriches the phase diagram, which now contains six types of evolutions.

In section 3 we proceed with the analysis of a more realistic universe, which includes radiation, baryonic matter and CDM. Further tests of the trajectories of type IIb and III are performed. In this setup we identify the initial (present) values for the tachyonic parameters characterizing the trajectories selected by SNIa data at 1σ confidence level. Then we achieve subsequent substantial reductions of this parameter region by successive inclusions of constraints from BAO, from the Hubble parameter data and from CMB acoustic scale. All these constraints refer to the cosmological evolution at background level.

In section 4 we develop a perturbative description at the linear level of the tachyonic scalar field, which is a prerequisite in deriving the CMB temperature power spectrum, also presented there. In the process the amount of CDM required in the tachyonic universe is found. Section 5 contains the concluding remarks.

We employ the system of units $c = 1$ and $8\pi G/3 = 1$. Throughout the paper the tachyonic parameter is fixed as $\mathsf{k} = 0.44$ and the present value of the Hubble parameter at $H_0 = 70.6$ km/sec/Mpc [17]-[19].

2 Background evolution of the flat Friedmann universe filled with tachyonic scalar field

In this section we present the background evolution of the universe dominated by a tachyonic scalar field with a special trigonometric potential.

2.1 Background dynamics and velocity phase diagram

We consider a flat Friedmann universe

$$ds^2 = dt^2 - a^2\,(t) \sum_\alpha (dx^\alpha)^2 \ , \tag{2.1}$$

(with x^α, $\alpha = 1, 2, 3$ the Cartesian coordinates and a the scale factor). The dynamics is governed by the Raychaudhuri (second Friedmann) equation

$$\dot{H} = -\frac{3}{2}\,(\rho + p) \tag{2.2}$$

and the continuity equation

$$\dot{\rho} + 3H\,(\rho + p) = 0 \ . \tag{2.3}$$

(Here $H \equiv \dot{a}/a$ is the Hubble parameter, ρ the energy density and p the pressure of the ideal fluid filling the universe, while a dot denotes derivatives with respect to the cosmological time t.) The (first) Friedmann equation

$$H^2 = \rho \tag{2.4}$$

stands as a first integral of the system (2.2)-(2.3).

The tachyonic Lagrangian is given by [20]

$$L = -V(T)\sqrt{1 - g^{ij}\,(\partial_i T)\,(\partial_j T)} \ , \tag{2.5}$$

where $V(T)$ is a potential. A spatially homogeneous scalar field $T(t)$ evolves according to

$$\frac{\dot{s}}{1 - s^2} + 3Hs + \frac{V_{,T}}{V} = 0 \ , \tag{2.6}$$

where $s = \dot{T}$ and $,T$ denotes the partial derivative with respect to T.

The energy-momentum tensor T_{ab} can be obtained from the variation of the action for tachyonic field with respect to the metric, and it can be decomposed with respect to an observer with 4-velocity u^a as

$$T_{ab} = \rho u_a u_b + 2q_{(a} u_{b)} - p h_{ab} + \pi_{ab} \ . \tag{2.7}$$

Here ρ, q_a, p and π_{ab} are the energy density, the energy current 3-vector, the isotropic pressure and the symmetric, trace-free, anisotropic pressure 3-tensor of the matter. With the choice $u_a = (dt)_a$ a spatially homogeneous tachyonic field becomes an ideal fluid ($q_a = 0$, $\pi_{ab} = 0$) with energy density

$$\rho^{(T)} = \frac{V(T)}{\sqrt{1 - s^2}} \ , \tag{2.8}$$

and pressure

$$p^{(T)} = -V(T)\sqrt{1 - s^2} \ . \tag{2.9}$$

As long as the potential is real, the Lagrangian density, $\rho^{(T)}$ and $p^{(T)}$ are well defined only for $s^2 \leq 1$. Outside this range the energy density and pressure remain well defined for an imaginary potential. Note that the fluid becomes effectively barotropic with the equation of state parameter $w_T = p^{(T)}/\rho^{(T)} = s^2 - 1$. Hence for subluminal ($s^2 < 1$) tachyonic

field evolutions $w_T < 0$ and (for a positive potential) the pressure is negative, allowing in principle for violations of the strong energy condition, rendering the tachyonic field into the dark energy regime. At $s^2 = 1$ the pressure vanishes, the fluid becoming dust.

We are interested in the dynamics generated by the simple trigonometric potential [8]:

$$V(T) = \frac{\Lambda\sqrt{1 - (1 + \mathsf{k})y^2}}{1 - y^2} , \qquad (2.10)$$

where

$$y = \cos\left[\frac{3}{2}\sqrt{\Lambda(1 + \mathsf{k})}\, T\right] \qquad (2.11)$$

is an alternative scalar field variable, while $\Lambda > 0$ and $-1 < \mathsf{k} < 1$ are the two parameters of the model. The system is invariant under the simultaneous parity changes

$$y \to -y , \quad s \to -s , \qquad (2.12)$$

which generates a double coverage of the dynamics of such a tachyon-filled universe in these velocity phase-space variables.

For numerical investigations it is worth to introduce the following dimensionless quantities [10]:

$$\hat{H} = \frac{H}{H_0}, \ \hat{V} = \frac{V}{H_0^2}, \ \Omega_\Lambda = \frac{\Lambda}{H_0^2}, \ \hat{T} = H_0 T , \qquad (2.13)$$

and the redshift z as independent variables. Then the equations of motion become

$$\hat{H}^2 = \frac{\hat{V}}{\sqrt{1 - s^2}} , \qquad (2.14)$$

$$\frac{dy}{dz} = \frac{3\sqrt{\Omega_\Lambda(1 + \mathsf{k})(1 - y^2)}}{2(1 + z)\hat{H}} s , \qquad (2.15)$$

$$\frac{1 + z}{1 - s^2}\frac{ds}{dz} = 3s + \frac{\hat{V}_{,\hat{T}}}{\hat{H}\hat{V}} , \qquad (2.16)$$

where $\hat{V}$ and $\hat{V}_{,\hat{T}}/\hat{V}$ are given by

$$\hat{V} = \frac{\Omega_\Lambda\sqrt{1 - (1 + \mathsf{k})y^2}}{1 - y^2} , \qquad (2.17)$$

$$\frac{\hat{V}_{,\hat{T}}}{\hat{V}} = \frac{3\sqrt{\Omega_\Lambda(1 + \mathsf{k})}\left[\mathsf{k} - 1 + (1 + \mathsf{k})y^2\right]}{2\sqrt{1 - y^2}\left[1 - (1 + \mathsf{k})y^2\right]} y . \qquad (2.18)$$

Since $\hat{H}(z = 0) = 1$, the first integral (2.14) gives a relation between the parameters: k, Ω_Λ, $y(z = 0) = y_0$ and $s(z = 0) = s_0$. The latter two parameters fix the initial conditions for the tachyonic scalar field. Remarkably, the equations (2.15) and (2.16) do not depend on Ω_Λ, as $\hat{H} \propto \sqrt{\Omega_\Lambda}$ and $\hat{V}_{,\hat{T}}/\hat{V} \propto \sqrt{\Omega_\Lambda}$ both hold. Therefore the diagram showing the evolutions in the $(\sqrt{\Omega_\Lambda}\hat{T} = \sqrt{\Lambda}T, s)$ or equivalently in the (y, s) planes for a given k and Ω_Λ will not dependent on the particular chosen value of Ω_Λ.

As shown on Fig. 1 the dynamics is quite rich. The attractive fix point in the center of the figure (corresponding to $y = 0$ and $s = 0$) represents the de Sitter evolution. Two types
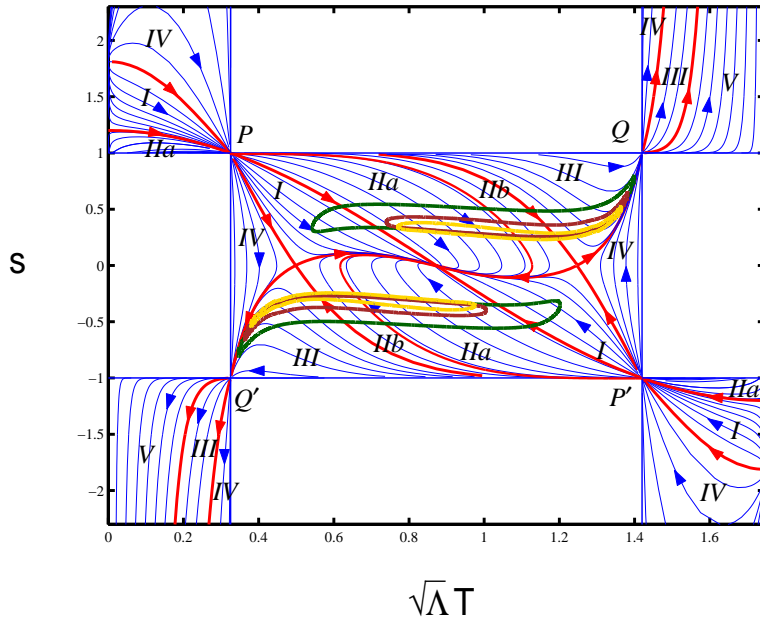
Figure 1. The velocity phase diagram of the tachyonic scalar field dominated universe, for a trigonometric potential and parameter $k = 0.44$. Compared to the early version of this phase diagram [8], [10] a new separatrix between IIa and IIb was added. The richness of the dynamics is encoded in the six types of distinct tachyonic evolutions. The de Sitter attractor is in the center of the figure while the soft singularities arise in the vertical stripes on both the upper right and the lower left corners. Two copies of all evolutions are consequence of the symmetry (2.12). Some of the evolutions cross the regions compatible at 1σ (68.3%) confidence level with i) SNIa data (delimited by a green contour), with ii) Hubble parameter data (yellow) and with iii) SNIa+Hubble parameter data (brown).

(I and II) of trajectories end in this de Sitter attractor, but they originate in different Big Bang singularities on the diagram. The evolutions of type I and the separatrices between the trajectories of types I and II start from the points $(y = \pm 1, s = \pm\sqrt{1 + 1/k})$, while type II from the lines $s^2 = 1$ [8]. For most of the trajectories arriving to any of the four corners (P, P', Q, Q') of the velocity phase diagram passage through the corners is allowed [8], as these are the only points on the horizontal lines ($s^2 = 1$), which do not represent singularities (the vanishing of the potential at $y = \pm(1 + k)^{-1/2}$ assures that $s = \pm 1$ does not imply an infinite energy density there). Nevertheless there is an exceptional trajectory for each corner point (given by a vanishing integration constant B in Eqs. (78) and (82) of [8]), which encounters a space-time singularity at the respective corner point. Inside the central rectangle the pressure is negative. In the side strips the pressure is positive, thus the expansion of the universe is slowing down in those regimes. There the field represents a pseudo-tachyon and has well-defined (real) Lagrangian, energy density and positive pressure. Since in the process

of evolving through the corners (forward in time at Q, Q' and backward in time at P, P') to the side strips both the potential V and $\sqrt{1-s^2}$ become imaginary, a redefined real potential $W(T) = iV(T)$ and $\sqrt{1-s^2} = i\sqrt{s^2-1}$ will be used in the Lagrangian[1], which then becomes $W(T)\sqrt{s^2-1}$. In this regime eventually a new type of soft cosmological singularity, the Big Brake is reached by the trajectories of type III, IV and V, at $y \to y_{BB}$ and $s^2 \to \infty$ [8], [10]-[12]. From among them two types (III and IV) also exhibit an evolution regime where the field has negative pressure. The trajectories of type III are again born on the lines $s^2 = 1$ with $p^{(T)} < 0$. The curves of type IV originate at the same points as those of type I, then they follows subsequent regimes with $p^{(T)} > 0$, then $p^{(T)} < 0$ and again $p^{(T)} > 0$, finally running into the Big Brake singularity. The separatrices between trajectories of type I and IV run into the unstable fix points $(y = \pm\sqrt{(1-\mathsf{k})/(1+\mathsf{k})}, s = 0)$ of the phase-velocity space [8]. The separatrices between the evolutions of type II and III, originating on the lines $s^2 = 1$ with $p^{(T)} < 0$ run into the same unstable fix points. From near the unstable fix points the trajectories either run into the de Sitter attractor or into a Big Brake singularity generating further separatrices between evolutions of type I and II or III and IV. The separatrices between the trajectories of type III and V have $p^{(T)} > 0$ and originate in Big Bang singularities at the corner points Q, Q', respectively. The trajectory of type V always has positive pressure.

On earlier versions of the velocity phase diagram (Fig. 1), discussed in Refs. [8], [10]-[12] it was not clear whether the separatrix between the evolutions of type II and III reaches the corner point P (P'). A thorough numerical investigation of the evolutions this time made it possible to answer this question. We confirmed that some of the evolutions of type II originate in the Big Bang type singularity lying outside the central rectangle, hence they evolve through positive pressures before they reach the corner point to pass in the rectangle region with negative pressure. These trajectories, denoted IIa on the velocity phase diagram however are complemented by other evolutions of type II, born in a Big Bang singularity lying on the horizontal boundary of the rectangle. Such trajectories, denoted IIb exhibit negative pressures throughout their evolution. The velocity phase diagram Fig. 1 includes now new separatrices between the trajectories of type IIa and IIb which originate in Big Bang singularities at the corner points P, P', respectively, inside the rectangle and both run into the de Sitter attractor. On the earlier version of the diagram it was also not clear how the diagram depends on the parameter Ω_Λ (or equivalently on Λ) which was fixed. We have clarified this by giving the diagram in variables independent of the actual value of Ω_Λ.

2.2 Confrontation with Supernovae Ia and Hubble parameter data

The cosmological test employing the supernovae data rely on the luminosity distance (d_L)-redshift relation. In a flat Friedmann universe the dimensionless luminosity distance $\hat{d}_L = H_0 d_L$ satisfies the relation

$$\left(\frac{\hat{d}_L}{1+z}\right)' = \frac{1}{\hat{H}} \ . \tag{2.19}$$

The confrontation of the tachyonic model with the Union 2.1 SNIa data set [14] is done through a χ^2-test, repeating the procedure of Ref. [10]. In this paper we also perform a

---

[1]When $W(T)$ is a constant, the pseudo-tachyon field degenerates into an anti-Chaplygin gas.

χ^2-test with the Hubble parameter-redshift relation by computing

$$\chi_H^2 = \sum_{i=1}^{30} \frac{\left[H_{th}\left(z_i \right) - \overline{H}_{obs}\left(z_i \right) \right]^2}{\sigma_i^2} \ . \tag{2.20}$$

Here $H_{th}\left(z_i \right)$ and $\overline{H}_{obs}\left(z_i \right)$ are the values of the Hubble parameter at redshifts z_i predicted by the cosmological model and determined from the observations, respectively, while σ_i is the scattering in $\overline{H}_{obs}\left(z_i \right)$. The data set on the Hubble parameter-redshift relation was given in Refs. [15] and [16]. Recently a subset of this data set was used to emphasize a tension with the ΛCDM model (by computing the two-point Omh^2 function) [21]. Finally, we perform a test with the combined SNIa and Hubble parameter data set by calculating $\chi_{SNIa+H}^2 = \chi_{SNIa}^2 + \chi_H^2$, where χ_{SNIa}^2 is the χ^2-value from the confrontation with SNIa data set.

The first integral (2.14) evaluated at $z = 0$ gives Ω_Λ (or equivalently Λ) as function of y_0, s_0. The confidence level contours resulted from the χ^2-tests are represented on the same velocity phase diagram (Fig. 1), which is independent of Ω_Λ. The SNIa test was not confronted with the velocity phase diagram in previous analyses. We found that the evolutions compatible with SNIa data at the 1σ confidence level are of the types I, II, and III only. The trajectories of type IV, which in principle could have allowed for accelerated expansion in recent times are disruled by SNIa data. The fact that the trajectories of type V could not produce accelerated expansion was obvious even without the SNIa test, as they do not venture into the rectangle region with negative pressure. The inclusion of the test with Hubble parameter-redshift relation shows that only the evolutions of types II and III fall within the 1σ confidence level.

2.3 Evolutions I and IIa disruled by nucleosynthesis and stability arguments

All evolutions surviving the SNIa test emerge from Big Bang like singularities, these however are different for the trajectories of type I, IIa, IIb and III. The past evolutions of these trajectories are depicted on Fig. 2. The trajectories compatible with the SNIa data, Hubble data and SNIa+Hubble data at 1σ confidence levels are represented by green, yellow and brown curves, respectively.

The evolutions of type I emerge from the singular point $y = \pm 1$, $s = \pm\sqrt{1 + 1/k}$ [8]. As shown on the upper right panel of Fig. 2, with increasing redshift the barotropic index $w_T = p^{(T)}/\rho^{(T)} = s^2 - 1$ increases monotonically and converges to $\mathsf{k}^{-1} \approx 2.273$, which is much larger as compared to the barotropic index of radiation. These trajectories then could not be consistent with Big Bang Nucleosynthesis (BBN), which stops when the plasma filling the Universe becomes dilute enough to reduce the number of collisions among nuclei and cooled down enough to stop the nuclei containing protons overcoming their electrostatic repulsion. This approximately happens at $T \approx 0.1$ MeV, which in the ΛCDM model corresponds to the redshift $z \approx 4 \times 10^8$. Due to the high pressure however BBN is longer in the tachyonic model of type I than in the ΛCDM model. In another line of reasoning, for high value of the barotropic index, the continuity equation yields

$$\rho_T \propto a^{-\frac{3}{k}(k+1)} \approx a^{-4.32} \ , \tag{2.21}$$

implying higher energy density of the tachyonic field close to the Big Bang, than for radiation, while the scale factor evolves as
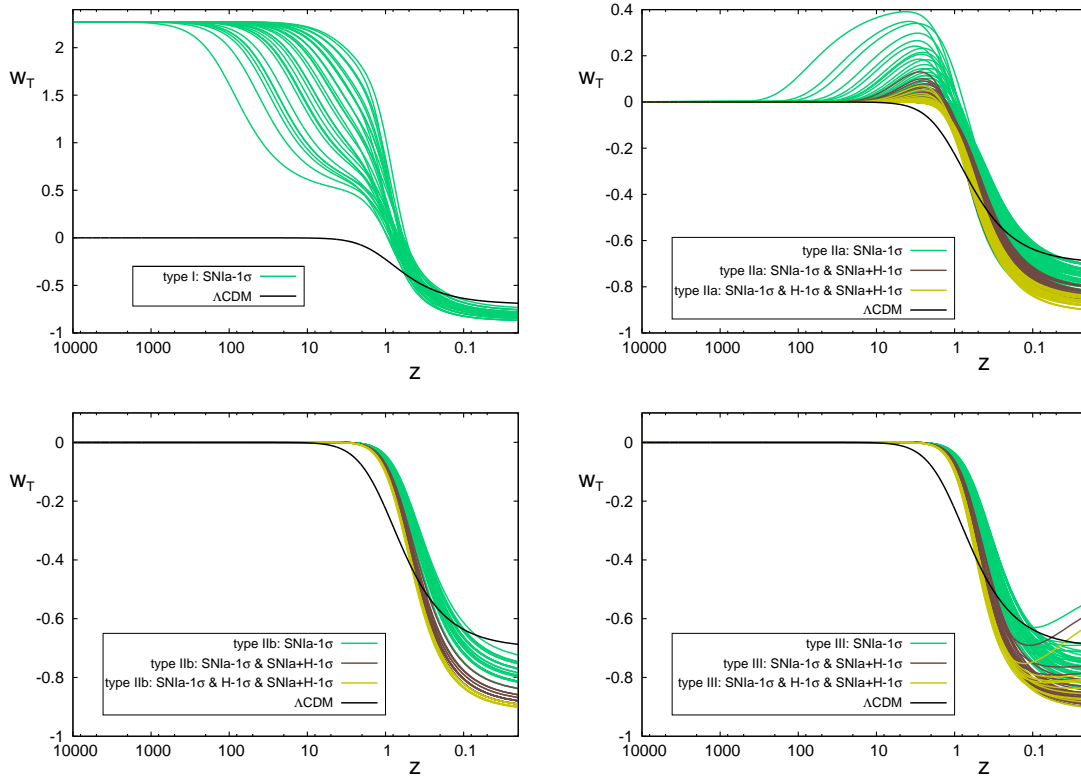
Figure 2. The distant past evolutions for different types of trajectories (type I on the upper left panel, type IIa on the upper right panel, type IIb on the lower left panel and type III on the lower right panel) fitting within 1σ confidence level with the Union 2.1 data set (green curves), with Hubble parameter data (yellow curves) and with SNIa+Hubble parameter data (brown curves). For comparison the evolution generated in the framework of the flat ΛCDM model with $\Omega_\Lambda = 0.7$ and $\Omega_m = 0.3$ is also shown.

$$a \propto t^{\frac{2k}{3(k+1)}} \approx t^{0.204} \ , \tag{2.22}$$

exhibiting a much slower expansion than in either a dust or a radiation dominated universe (where $a \propto t^{2/3}$ and $a \propto t^{1/2}$, respectively). All of these suggest that by the end of the BBN the evolution (2.22) would have resulted in a higher ratio of the nuclei with large mass numbers compared to Hydrogen as in a radiation dominated universe. As the predictions of an early radiation dominated universe are consistent with observations of the abundances of primordial light elements (D, ^{3}He, ^{4}He, ^{7}Li) [22], type I trajectories can be considered disruled.

Similar considerations disrule those evolutions of type IIa which run very close to the separatrix between the evolutions of type I and IIa, as they also build up large pressures (see Figs. 1). For these evolutions, once the universe passes the corner points, the pressure starts to increase again, driving them away from the dust-dominated evolutions. The evolutions presenting such pressure humps are however significantly disruled by the combined SNIa test and Hubble parameter data.

Another aspect to comment on would be that outside the rectangle, inside the stripes the pseudo-tachyonic field has a negative speed of sound squared. Indeed, the pressure is

growing when the energy density is decreasing, hence, the derivative of the pressure with respect to energy density is negative. The presence of an imaginary sound velocity means that the second order equation governing the evolution of the perturbations instead of oscillatory solutions exhibits two solutions with real exponents, one of them positive, the other negative [23]. The positive one corresponds to an exponentially growing mode, a Laplacian instability in the evolution of the perturbations. Hence we disrule the models allowing for such instabilities in the past. Note that the very same argument disrules once again the evolutions of type I.

By contrast the trajectories of type IIb and III allow for a dark matter dominated past ($w_T \approx 0$, see Fig. 2), as they asymptote to the singular horizontal lines of the velocity phase diagram Fig. 1 and they never get away from there once they approach it. With a (today insignificant) radiation component added, at the background level these trajectories could be consistent with the early evolution of the Universe (with radiation dominating at high redshift) and there are no instabilities arise in the past either.

3   Cosmological tests of an enhanced tachyonic universe at the background level

In order to confront with various cosmological observations we need to make the model more realistic. In the following subsection we introduce such an enhanced model, while in the second subsection we perform a series of cosmological tests available at background level, e.g. without working out the perturbation formalism.

3.1   Tachyonic universe encompassing radiation, baryons and CDM

Starting from this subsection we include radiation, baryonic matter and CDM in the model. In the flat ΛCDM model a detailed analysis of temperature power spectrum of the cosmic microwave background shows that the locations and the heights of the acoustic peaks are sensitive to $\Omega_b h^2$ [24]. We fix the baryonic matter contribution as $\Omega_b h^2 = 0.022161$ cf. the Planck collaboration (taken from the last column of Table 5 of Ref. [18]). In the late universe the energy density of the baryonic matter and of radiation are negligible as compared to the density of dark energy. Anticipating the result of Section 4, based on a perturbative analysis and CMB temperature power spectrum, we also include CDM with $\Omega_{CDM} = 0.22$.

In the presence of radiation, baryonic matter and CDM components, from among the equations (2.14)-(2.16) only (2.14) is changed:

$$\hat{H}^2 = \frac{\hat{V}}{\sqrt{1-s^2}} + (\Omega_b + \Omega_{CDM})(1+z)^3 + \Omega_{rad}(1+z)^4 , \qquad (3.1)$$

where Ω_{rad} is the radiation component (electromagnetic radiation and massless neutrinos). The symmetry (2.12) of the system continues to hold. However since $\hat{H}$ is not proportional to $\sqrt{\Omega_\Lambda}$, in contrast with the pure tachyonic model, the tachyonic field equations (2.15)-(2.16) are sensitive to Ω_Λ. Therefore the initial conditions fixed by y_0, s_0 cannot be represented on a single velocity phase diagram, in general different pairs of y_0, s_0 would generate different Ω_Λ-s through Eq. (3.1), evaluated at $z = 0$.

On Fig. 3 we represented the initial data for the evolutions of type IIb and III in the parameter space (y_0,s_0). Blue and green dots denote the set of initial conditions at $z = 0$ for the evolutions of type IIb originating from Big Bang type singularities lying on the lines
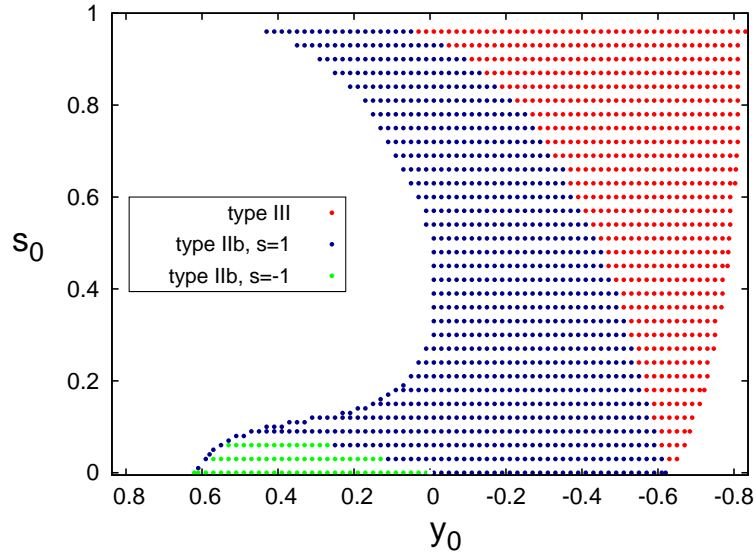
Figure 3. The initial conditions at $z = 0$ for evolutions of type IIb (blue and green dots) and III (red dots) in the parameter space (y_0, s_0). The trajectories of type IIb originate from Big Bang type singularities lying on the lines $s = 1$ (blue dots) or $s = -1$ (green dots).

$s = 1$ and $s = -1$, respectively. The red dots represent initial conditions for the evolutions of type III. Due to the symmetry (2.12), only the region $s_0 \geq 1$ is shown. In the rest of this section we will restrict these domains by confrontation with various cosmological tests.

3.2 SNIa, BAO distance ratios, Hubble parameter and CMB acoustic scale tests

We will confront the enhanced tachyonic model with both the SNIa and Hubble parameter data in a similar manner as described in the subsection 2.2 for the pure tachyonic model. We will also test the model with BAO data, which determine the ratio:

$$d_z\left(z\right) = \frac{r_s\left(z_{drag}\right)}{D_V\left(z\right)} \ , \tag{3.2}$$

at different redshifts. Here $D_V\left(z\right)$ is the volume distance:

$$D_V^3\left(z\right) = \frac{zD_A^2\left(z\right)}{H\left(z\right)} \ , \tag{3.3}$$

with comoving angular diameter $D_A\left(z\right)$ which can be expressed by the luminosity distance as

$$D_A\left(z\right) = \frac{d_L\left(z\right)}{1+z} \ . \tag{3.4}$$

The quantity r_s denotes the sound horizon:

$$r_s\left(z\right) = \int_z^\infty \frac{dz'}{H\sqrt{3\left(1+R\right)}} \ , \tag{3.5}$$

with $R = 3\rho_b/4\rho_\gamma$, where ρ_b and ρ_γ are the energy densities of the baryons and photons, respectively. The sound horizon in (3.2) is evaluated at the baryon drag epoch (z_{drag}) when

the baryon velocity perturbations decouple from the photon dipole $q_a^{(\gamma)}$. This happens approximately when the baryon drag optical depth

$$\tau_{drag}(z) = \int_0^z \frac{n_e \sigma_T}{(1+z') HR} dz' \tag{3.6}$$

reaches unity $(\tau_{drag}(z_{drag}) = 1)$ [25], [26]. Here n_e is the number density of free electrons (without reionization history) and σ_T is the Thompson cross section. The determination of z_{drag} requires to know $n_e(z)$ from some recombination model. We compute z_{drag} and $r_s(z_{drag})$ numerically from a modified version of the CAMB code [26], [27], [28] in which we implemented the evolution of the tachyonic universe. For modeling the recombination history we used the RECFAST subcode [29].

Six data on BAO and their inverse covariance matrix C^{-1} applied in the analysis are given by Table 3 of Ref. [30] and by Eq. (4.3) of Ref. [31], respectively. From the theoretically derived $d_z^{th}(z_i)$ $(i = 1,..,6)$ and from the observations $d_z^{obs}(z_i)$ a six dimensional vector $\mathbf{X}$ is constructed containing $d_z^{th}(z_i) - d_z^{obs}(z_i)$ in its ith row. In the cosmological test of the enhanced tachyonic universe model we computed

$$\chi_{BAO_1}^2 = \mathbf{X}^T C^{-1} \mathbf{X} , \tag{3.7}$$

where T denotes the transposed vector. We also include the Baryon Oscillation Spectroscopic Survey [32] result $d_z(0.57) = 0.0731 \pm 0.0018$ [33] by defining

$$\chi_{BAO}^2 = \chi_{BAO_1}^2 + \left(\frac{d_z^{th}(0.57) - 0.0731}{0.0018} \right)^2 . \tag{3.8}$$

Before decoupling the acoustic oscillations in a baryon-photon plasma induce an oscillatory pattern in the CMB temperature. For adiabatic fluctuations, the mth Doppler peak has comoving wave number $k_m = m\pi/r_s(z_*)$ [34]. Here z_* is the redshift when the photons decouple from baryons, i.e. when

$$\tau(z) = \int_0^z \frac{n_e \sigma_T}{(1+z') H} dz' \tag{3.9}$$

reaches unity $(\tau(z_*) = 1)$. The location of the first peak of the CMB temperature spectrum in multipole space is

$$l_A \approx \frac{\pi D_A(z_*)}{r_s(z_*)} . \tag{3.10}$$

We test the tachyonic universe model with the CMB acoustic scale $l_A^{obs} = 301.65 \pm 0.18$ [35] by computing the following χ^2 value:

$$\chi_{CMB}^2 = \left(\frac{l_A^{th} - 301.65}{0.18} \right)^2 , \tag{3.11}$$

where l_A^{th} is derived numerically by the modified CAMB code.

On Fig. 4 the regions of parameter space (y_0, s_0) are shown in which the tachyonic universe model fits with the above data sets at 1σ confidence level. On each panel the yellow curve separates the regions of initial conditions for trajectories of types IIb (on the left) and III (on the right). On the upper left panel the colored regions represent the fitting of the
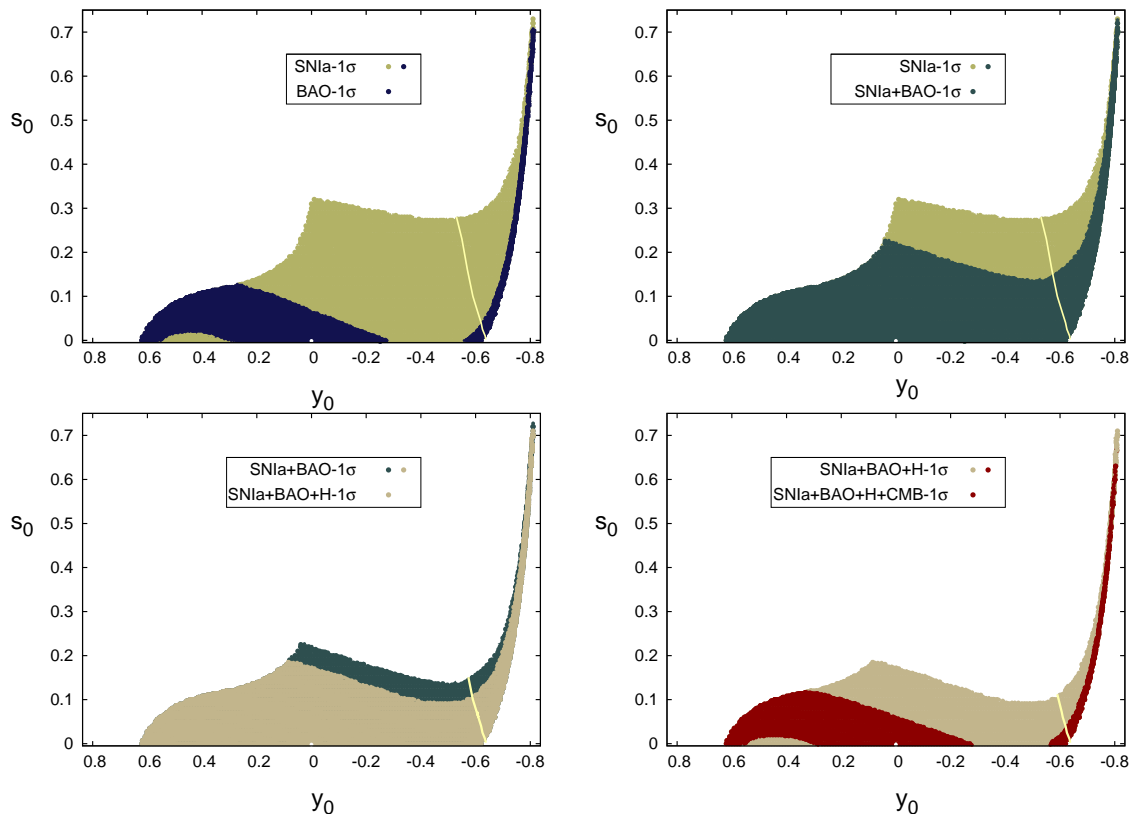
Figure 4. The initial values (y_0, s_0) of the tachyonic parameter space constrained by cosmological tests. Upper left panel: the 1σ confidence level regions selected by the SNIa (mint green) and by BAO (navy blue), the latter masking out some of the more extended SNIa 1σ region. Upper right: the inclusion of BAO reduces the 1σ confidence level region of the SNIa (mint green) to the one of the SNIa+BAO (myrtle green). Lower left: the inclusion of Hubble parameter data set further reduces the 1σ confidence level region of the SNIa+BAO (myrtle green) to the one of SNIa+BAO+H (ecru). Lower right: the inclusion of CMB acoustic scale reduces once again the 1σ confidence level region of the SNIa+BAO+H (ecru) to the one of SNIa+BAO+H+CMB (crimson red). All 1σ parameter regions are divided into a left region (representing type IIb trajectories) and a right region (representing type III trajectories) by a yellow line. The ΛCDM attractor in the origin is represented by a white dot.

model at 1σ confidence level with SNIa (both the mint green and navy blue regions) and BAO (the navy blue region) data sets. The BAO distance ratio test leads to a much stringent restriction of the parameter space than the SNIa test. However we note that the BAO data set consists of much less data (7) than the SNIa set (580), and the χ^2-test works better for a larger number of data points. On the subsequent three panels we show how the inclusion of each of the BAO distance ratios, Hubble parameter-redshift relation and CMB acoustic scale cosmological test successively restrict the 1σ region of the SN1a test.

In particular, on the upper right panel the subset of the SNIa-1σ domain which fits to the SNIa+BAO data set at 1σ confidence level is shown in myrtle green. This combined test was performed by computing $\chi^2_{SNIa+BAO} = \chi^2_{SNIa} + \chi^2_{BAO}$. The SNIa+BAO test is less restrictive as compared with the test of BAO only, since the BAO-1σ domain is included into the SNIa-1σ domain and the critical χ^2 belonging to the 1σ confidence level increases with the amount of data. Since the SNIa test is based on a significantly larger amount of data than the number

of BAO distance ratios, the fitting with SNIa data dominates the combined test. On the lower left panel the 1σ confidence region resulted from the $\chi^2_{SNIa+BAO+H} = \chi^2_{SNIa}+\chi^2_{BAO}+\chi^2_H$ test with the Hubble parameter data set also included is shown in ecru. Finally, we add the CMB acoustic scale to the test by calculating $\chi^2_{SNIa+BAO+H+CMB} = \chi^2_{SNIa} + \chi^2_{BAO} + \chi^2_H + \chi^2_{CMB}$ which further restricts the domain of the parameter space which fits at 1σ confidence level, shown in crimson red on the lower right panel. This is quite similar in shape and size to the BAO-1σ domain.

The tale of Fig. 4 is that there are trajectories of both types IIb and III which survive the various combined tests. By comparing Figs. 3 and 4 we conclude that a relatively larger subset of evolutions of type IIb fit the data at 1σ confidence level as compared to the trajectories of type III. In this sense, from the two possible future scenarios, the evolutions ending in de Sitter attractor are more likely.

4   Cosmic microwave background in type IIb and III tachyonic universe models

In this section we perturb the flat Friedmann universe in order to derive the CMB temperature spectrum. As usual the perturbations of the Friedmann universe are classified into scalar, vector and tensor types. Here we investigate only the scalar type perturbations by implementing the source terms due to perturbations of the tachyonic scalar field and their evolution equations into the freely available CAMB code.

The perturbation equations in the CAMB code were derived in the framework of 3+1 covariant formalism [26],[27], [36], [37] in which the space-time metric g_{ab} is split in the form $g_{ab} = u_a u_b + h_{ab}$, with $u^a u_a = 1$ and $u^a h_{ab} = 0$. Here h_{ab} is the projection tensor into the rest space of an observer moving with 4-velocity u^a. In the Friedmann space-time a convenient choice is $u_a = (dt)_a$ which is the comoving system with the matter flow. In the perturbed Friedmann space-time there are infinite possible choices for u_a which coincide with $(dt)_a$ in the absence of perturbations. In the CAMB code for the scalar type perturbation the frame (i.e. u_a) is defined by $A_b = u^b \nabla_b u_a = 0$, where ∇_a is the covariant derivative. The scalar type velocity perturbations of the CDM vanish in this so called CDM frame. This description of the perturbations corresponds to the choice of synchronous gauge in a metric based perturbation formalism [38].

The tachyonic scalar field interacts with the other matter components only gravitationally. Therefore the contributions arising from the tachyonic field to the equations governing the perturbations of other matter components appear exclusively through the changes induced in the space-time curvature. In other words no particle scattering processes between the tachyonic and other matter components are allowed. In the 3+1 covariant formalism the energy-momentum tensor of the perturbed matter is described in terms of $D_a \rho$, $D_a p$, q and π_{ab}. After we will enlist the contributions of the tachyonic field, we will derive the evolution equations governing the perturbations.

The tachyonic energy-momentum tensor, as arising from the variation of its action with respect to the metric, and applying the decomposition (2.7) leads to

$$\rho^{(T)} = V\sqrt{1-2X} + \frac{V\dot{T}^2}{\sqrt{1-2X}} \ ,$$

$$p^{(T)} = -\frac{V\left(D^a T\right)\left(D_a T\right)}{3\sqrt{1-2X}} - V\sqrt{1-2X} \ ,$$

$$q_a^{(T)} = \frac{V\dot{T}D_aT}{\sqrt{1-2X}} \ ,$$

$$\pi_{ab}^{(T)} = \frac{V\left(D_{\langle a}T\right)\left(D_{b\rangle}T\right)}{\sqrt{1-2X}} \ . \tag{4.1}$$

where

$$X = \frac{1}{2}\left(\nabla^aT\right)\left(\nabla_aT\right) \ , \tag{4.2}$$

D_a is the covariant derivative on the 3-space with metric h_{ab} $(D_aT = h_a^b\nabla_bT)$ and the dot denotes: $\dot{T} = u^a\nabla_aT$ (in the absence of perturbations this coincides with the time derivative employed at the background level). The angular bracket $\langle\ \rangle$ on abstract indices denotes the trace free part of a symmetrized tensor projected in all indices with the metric h_{ab}.

The 3+1 covariant equations governing the perturbations at first order contain the background values of $\rho^{(T)}$ and $p^{(T)}$, their spacelike derivatives $(D_a\rho^{(T)}$ and $D_ap^{(T)})$ and also the quantities $q_a^{(T)}$ and $\pi_{ab}^{(T)}$. At first order in the perturbations we find

$$D_a\rho^{(T)} = \frac{Vs}{(1-s^2)^{3/2}}D_a\dot{T} + \frac{V_{,T}}{\sqrt{1-s^2}}D_aT \ ,$$

$$D_ap^{(T)} = \frac{Vs}{\sqrt{1-s^2}}D_a\dot{T} - \sqrt{1-s^2}V_{,T}D_aT \ ,$$

$$q_a^{(T)} = \frac{Vs}{\sqrt{1-s^2}}D_aT \ , \quad \pi_{ab}^{(T)} = 0 \ . \tag{4.3}$$

Here s denotes the background value of $\dot{T}$. From the three nonvanishing quantities describing the perturbed field only two are independent since the pressure gradient can be expressed as

$$D_ap^{(T)} = \left(1-s^2\right)\left[D_a\rho^{(T)} - \frac{2V_{,T}}{Vs}q_a^{(T)}\right] \ . \tag{4.4}$$

In what follows we apply a harmonic expansion in order to derive ordinary differential equations for the variables characterizing the perturbation in Friedmann space-time. The scalar harmonics are the eigenfunctions of the spatial Laplacian:

$$D^2Q^{S(k)} = \frac{k^2}{a^2}Q^{S(k)} \ , \tag{4.5}$$

with $\dot{Q}^{S(k)} = 0$ at zeroth order. From $Q^{S(k)}$ we construct the following projected vector and symmetric trace-free tensor:

$$Q_a^{S(k)} = \frac{a}{k}D_aQ^{S(k)} \ , \quad Q_{ab}^{S(k)} = \frac{a^2}{k^2}D_{\langle a}D_{b\rangle}Q^{S(k)} \ . \tag{4.6}$$

The 3-vectors and symmetric trace-free 3-tensors arising from scalar perturbations can be expanded in terms of $Q_a^{S(k)}$ and $Q_{ab}^{S(k)}$, respectively [26], [37]. The harmonic expansions for the tachyonic field variables are

$$\delta_a^{(T)} \equiv \frac{a}{\rho^{(T)}}D_a\rho^{(T)} = \sum_k k\delta_k^{(T)}Q_a^{S(k)} \ , \tag{4.7}$$

$$D_a p^{(T)} = \rho^{(T)} \sum_k \frac{k}{a} p_k^{(T)} Q_a^{S(k)} \;, \tag{4.8}$$

$$q_a^{(T)} = \left(\rho^{(T)} + p^{(T)} \right) \sum_k v_k^{(T)} Q_a^{S(k)} \;. \tag{4.9}$$

Defining the expansion of $D_a T$ as

$$D_a T = \sum_k \frac{k}{a} T_k Q_a^{S(k)} \;, \tag{4.10}$$

we find

$$v_k^{(T)} = \frac{k}{as} T_k \;, \tag{4.11}$$

$$\delta_k^{(T)} = \frac{s}{1 - s^2} \dot{T}_k + \frac{V_{,T}}{V} T_k \;, \tag{4.12}$$

where we have used the commutation relation: $a D_a \dot{T} = (a D_a T)^{\cdot}$ which is valid in the CDM frame. The harmonic coefficient $(p_k^{(T)})$ arises from harmonic decomposition of Eq. (4.4):

$$p_k^{(T)} = \left(1 - s^2\right) \left[\delta_k^{(T)} - \frac{2V_{,T}}{V} \frac{as}{k} v_k^{(T)} \right] \;. \tag{4.13}$$

The equations of motion for $v_k^{(T)}$ and $\delta_k^{(T)}$ follow from the divergenceless condition of the energy-momentum tensor for tachyonic field $(\nabla^a T_{ab}^{(T)} = 0)$ and a harmonic expansion. Taking the 3-gradient of the projection $u^b \nabla^a T_{ab}^{(T)} = 0$ gives the evolution equation for $\delta_a^{(T)}$, while the equation governing $q_a^{(T)}$ emerges from the projection $h_c^b \nabla^a T_{ab}^{(T)} = 0$. Then the harmonic expansion generates the equations of motion for $v_k^{(T)}$ and $\delta_k^{(T)}$.

At this point it is worth to introduce the variable

$$\mathcal{X}_k^{(T)} = k \delta_k^{(T)} + 3aHs^2 v_k^{(T)} = \frac{ks^2}{1 - s^2} \left(\frac{T_k}{s} \right)^{\cdot} \tag{4.14}$$

replacing $\delta_k^{(T)}$, as the evolution equation for $\mathcal{X}_k^{(T)}$ becomes simpler. For the second equality of (4.14) we have employed Eq. (2.6). Note that the original Fourier components $\left(T_k, \dot{T}_k \right)$ of the velocity phase-space variables originally replaced by $\left(v_k^{(T)}, \delta_k^{(T)} \right)$ are changed into $\left(v_k^{(T)}, \mathcal{X}_k^{(T)} \right)$.

The equations of motion for the tachyonic scalar field perturbations in the Fourier space read

$$v_k^{(T)\prime} = -\mathcal{H} v_k^{(T)} + \frac{1 - s^2}{s^2} \mathcal{X}_k^{(T)} \;, \tag{4.15}$$

$$\mathcal{X}_k^{(T)\prime} = -3 \left(1 - s^2\right) \mathcal{H} \mathcal{X}_k^{(T)} - k^2 s^2 \left(\mathcal{Z}_k + v_k^{(T)} \right)$$
$$+ 3s^2 \left(\mathcal{H}' - \mathcal{H}^2 \right) v_k^{(T)} \;, \tag{4.16}$$

where $\mathcal{H} = a'/a$ and the prime denotes the derivative with respect to the conformal time η introduced as $ad\eta = dt$. The variable $\mathcal{Z}_k$ determines the harmonic coefficient of the comoving

spatial gradient of the expansion $\Theta = D^a u_a$ ($= 3H$ in the unperturbed Friedmann space-time) as

$$\mathcal{Z}_a \equiv aD_a\Theta = \sum_k \frac{k^2}{a}\mathcal{Z}_k Q_a^{S(k)} \ . \qquad (4.17)$$

By virtue of the definitions (4.11) and (4.14) the equation (4.15) is identically satisfied, while Eq. (4.16) gives the following second order equation for T_k:

$$\left(\frac{\dot{T}_k}{1-s^2}\right)^{\cdot} = -3H\dot{T}_k - \left[\left(\frac{V_{,T}}{V}\right)_{,T} + \frac{k^2}{a^2}\right]aT_k - ks\mathcal{Z}_k \ . \qquad (4.18)$$

This equation can also be derived directly from the action for the tachyonic scalar field, at linear older in the perturbations.
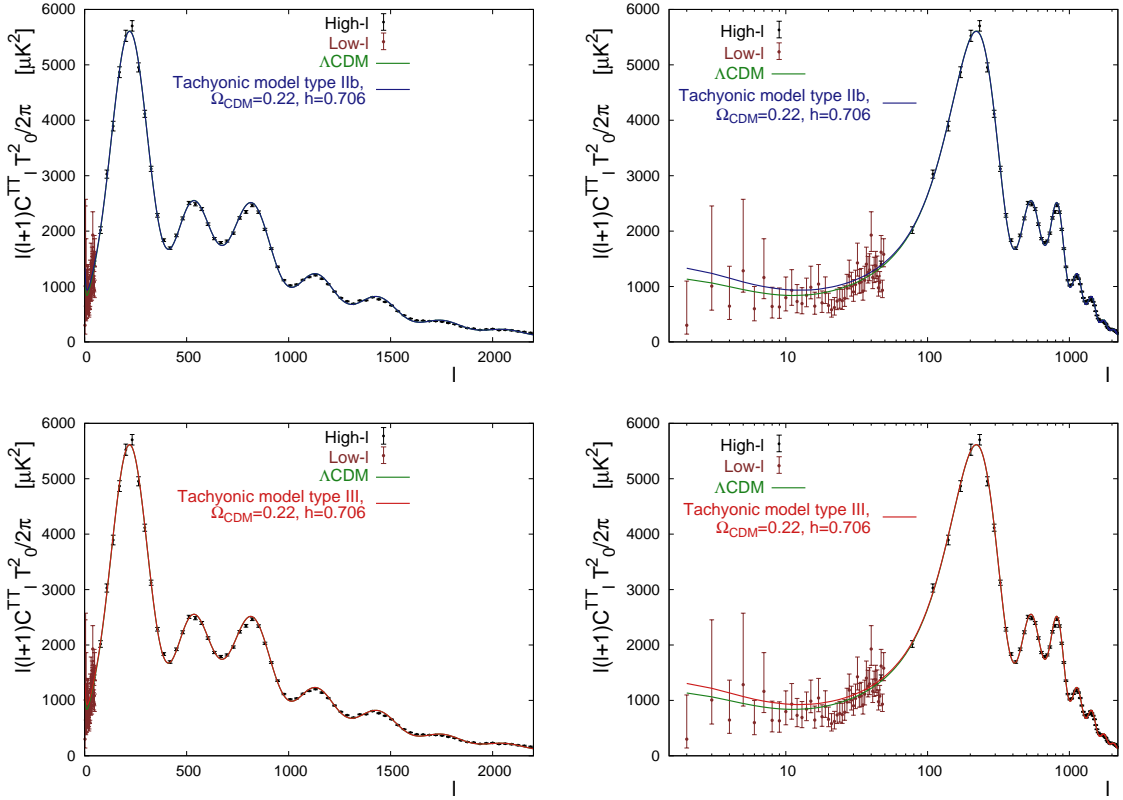

Figure 5. The CMB temperature power spectrums is shown for evolutions of type IIb (upper row, blue line) and III (lower row, red line) on linear multipole l scale (left columns) and logarithmic scale (right columns). The green line represents the best fit ΛCDM model (its parameters are given by the last column in Table 5 of [18]). Data points with error bars are shown with brown for Low$-l$ and black for High$-l$ multipoles.

At high redshift $s^2 \approx 1$, the tachyonic scalar field behaves as CDM, therefore we can choose the same adiabatic initial conditions as for CDM at $z \approx 10^9$. The parameters such as the Thompson scattering optical depth due to reionization τ, the scalar spectral index n_s, the power of the primordial scalar curvature perturbation A_s are taken from the ΛCDM model (the last column in Table 5 of [18]). Other parameters affecting the CMB temperature power spectrum are H_0, Ω_b and Ω_{CDM}. From among these we already fixed the first two.

By varying the last one over the range $\Omega_{CDM} \in (0, 0.3)$ we found the most reasonable CMB temperature power spectrum for the value of $\Omega_{CDM} = 0.22$ for either type of evolutions. On Fig. 5 we represented the best fit CMB temperature power spectrum for the evolutions of type IIb (upper row, blue line) and III (lower row, red line) on linear multipole l scale (left columns) and logarithmic scale (right columns). For comparison the green line representing the best fit ΛCDM model is also shown. The data set and their error bars are given in brown for Low$-l$ and black for High$-l$ multipoles. The CMB spectrum in the tachyonic universe model fits the Planck data as well as the standard ΛCDM model at high multipoles. At low multipoles the power is somewhat higher than in the case of the ΛCDM model.

5 Concluding Remarks

We investigated a tachyonic scalar field model governed by a trigonometric potential, which exhibits a rich variety of future evolutions, depending on the initial data and the actual value of the model parameters. For a positive model parameter $k = 0.44$ chosen for this paper, all possible evolutions originate in Big Bang type singularities, while they end either in a de Sitter exponential expansion (trajectories of type I and II) or into a sudden future singularity (types III, IV and V).

Previous confrontation with SNIa data confirmed that despite so different, both future scenarios are compatible with the hypothesis of dark energy in the form of this tachyonic scalar field. It this paper we clarified which types are allowed by observations. Type V evolutions being confined to the positive pressure regions, never achieve accelerated expansion, hence they are excluded. A careful analysis of the model of a Friedmann universe filled with the tachyonic scalar field identified that all evolutions compatible with the Union 2.1 SNIa data are of types I, II and III only, those of type IV running outside the 1σ contours of the SNIa test. Furthermore, the Hubble parameter data set test revealed that while at 1σ confidence level the trajectories of types II and III remain compatible, the trajectories of type I are disruled.

On the other hand, the negative pressure of the tachyonic scalar field decreases fast in magnitude during the backward evolution in time of the trajectories of types I-III. The past behavior of the evolutions of type II was not well understood before. Indeed, it was unclear whether the separatrix between the evolutions of type II and III reaches the corner point P (P'), in other words whether there are evolutions of type II with eternal negative pressure. Our present analysis has elucidated that such evolutions are possible, leading to a further subclassification of the trajectories of type II into the subtype IIa (trajectories born from a Big Bang with positive pressure, evolving superluminally, then passing through the corner point P (P') and becoming dark energy with negative pressure nowadays) and IIb (born from a Big Bang with negative pressure). A new separatrix between these subtypes IIa and IIb, starting from the point P (P') was added to the velocity phase diagram, Fig. 1.

Both evolutions of types IIb and III become dust-like in the past, suggesting a degeneration into dark matter of the dark energy scalar field. By contrast the trajectories of type I and some of those of IIa exhibit a large build-up of pressure in the distant past, disruling them as viable cosmological models explaining BBN. Another immediate argument for invalidating the evolutions of type I and all evolutions of type IIa is a negative speed of sound squared in the regions with positive pressure, which in general leads to instabilities in the evolution of perturbations. Such instabilities would not allow the universe to reach its present state. (Similar instabilities could drastically affect the future evolution of the trajectories of type

III, such that they would be hampered to reach the soft singularities. Such a discussion falls beyond the scope of the present paper.) As the evolutions IIb and III are both compatible with the SNIa and Hubble parameter data sets and they do not suffer from instabilities, a more thorough analysis of these evolutions has been performed in the rest of the paper.

In order to get a viable cosmological model, radiation, baryonic matter and CDM constituents were included into the model, complementing the dominant tachyonic scalar field. Then the evolutions of type IIb and III of this 4-component model were confronted with a series of cosmological tests at the background level, including the supernova type Ia Union 2.1 data, BAO distance ratios, the Hubble parameter data and the CMB acoustic scale. We identified the evolutions of both types, which at 1σ confidence level survive these cosmological tests.
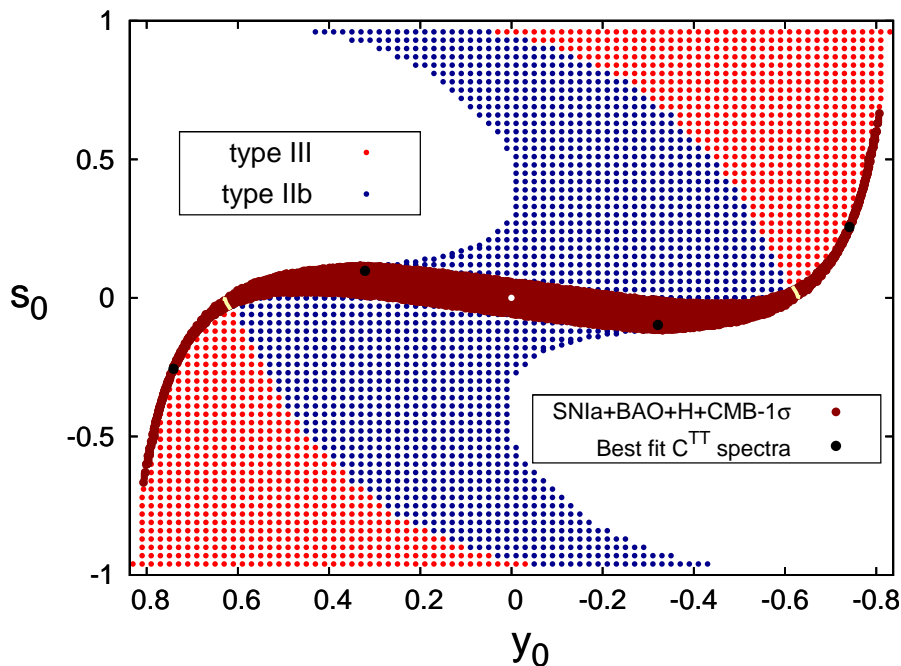

Figure 6. The initial conditions (at $z = 0$) in the parameter space (y_0, s_0) for the evolutions of type IIb (blue dots) and III (red dots), as restricted by the combined cosmological test of the SNIa data, BAO distance ratios, Hubble parameter data and CMB acoustic scale, evaluated for $\Omega_{CDM} = 0.22$. The initial data where the CMB temperature power spectrum showed the best fit for each type of evolution is indicated by black bullets. The ΛCDM attractor in the origin is represented by a white dot. Although the points (y_0, s_0) and $(-y_0, -s_0)$ represent identical tachyonic trajectories, both are shown in order to obtain a continuos parameter domain (crimson red) compatible with the combined test at 1σ confidence level.

A further test of the model evolutions was performed at perturbative level. There we derived the CMB temperature power spectrum and found the best agreement with the Planck data for a CDM component with $\Omega_{CDM} = 0.22$, less than in the ΛCDM model. The difference in the amount of CDM is explained by the dust-like behaviour of the tachyonic scalar field. The fit of the spectrum with the data was similar to the ΛCDM model at high multipoles, but the power remained slightly overestimated at low multipoles, for both types of evolutions. There, however, the fit of the ΛCDM model is also less satisfactory than for the high multipoles, and any future improvement on the ΛCDM model to address this could

also improve the fit of the tachyonic model.

In standard cosmology the SNIa test, BAO distance ratios and the location of the first peak of the CDM temperature power spectrum generate transverse 1σ contours. In our analysis we have assumed a flat Friedmann background and the CDM temperature power spectrum selected $\Omega_{CDM} = 0.22$, hence the rest of the tests could be used to restrict the tachyonic parameters. The result was presented on Fig. 4: the 1σ domain of the SNIa test was severely restricted by BAO distance ratios, this was successively further reduced by the Hubble parameter data set and finally by the CMB acoustic scale. The subset of evolutions of types IIb and III compatible at 1σ confidence level with these combined tests as compared to the full set of evolutions of types IIb and III are shown on Fig. 6. A relatively larger subset of the type IIb evolutions (towards the de Sitter attractor) survive the combined tests, as compared to the similar evolutions of type III (converging to a future soft singularity).

In summary we found that a tachyonic scalar field universe enhanced with radiation, baryonic matter and CDM constituents could well harmonize with the enlisted observations of our physical universe and the parameter space of the model compatible with these tests allows for two types of evolutions. These run similarly in the past, both being born from a Big Bang, with a subsequent dust-like evolution of the scalar field, achieving scalar field dark energy driven acceleration at present, but diverging in their future either into the de Sitter type expansion (type IIb) or by contrast, reaching a positive pressure regime, leading to a sudden future singularity (type III). How seriously the latter evolutions would be hampered by instabilities after crossing the positive pressure divide (the cornerstone P of the phase diagram) remains a question for future analysis.

Acknowledgements

References

[1] A. G. Riess, A. V. Filippenko, P. Challis et al., *Observational Evidence from Supernovae for an Accelerating Universe and a Cosmological Constant*, Astron. J. **116**, 1009 (1998) [astro-ph/9805201];
S. J. Perlmutter, G. Aldering, G. Goldhaber et al., *Measurements of Omega and Lambda from 42 High-Redshift Supernovae*, Astroph. J. **517**, 565 (1999) [astro-ph/9812133].

[2] Y. Fujii, *Origin of the gravitational constant and particle masses in a scale-invariant scalar-tensor theory*, Phys. Rev. D **26**, 2580 (1982);
L. H. Ford, *Cosmological-constant damping by unstable scalar fields*, Phys. Rev. D **35**, 2339 (1987);
C. Wetterich, *Cosmology and the fate of dilatation symmetry*, Nucl. Phys B. **302**, 668 (1988);
T. Chiba, N. Sugiyama and T. Nakamura, *Cosmology with x-matter*, Mon. Not. Roy. Astron. Soc. **289**, L5 (1997) [astro-ph/9704199];
P. G. Ferreira and M. Joyce, *Structure formation with a self-tuning scalar field*, Phys. Rev. Lett. **79**, 4740 (1997) [astro-ph/9707286];
R. R. Caldwell, R. Dave and P. J. Stein- hardt, *Cosmological Imprint of an Energy Component with General Equation of State*, Phys. Rev. Lett. **80**, 1582 (1998) [astro-ph/9708069];

Cs. Csáki, N. Kaloper and J. Terning, *The Accelerated Acceleration of the Universe*, J. Cosmol. Astropart. Phys. (JCAP) **06**, 022 (2006) [astro-ph/0507148];
S. Tsujikawa, *Quintessence: A Review*, Class. Quantum Grav. **30**, 214003 (2013) [arXiv:1304.1961 [gr-qc]].

[3] C. Armendariz-Picon, T. Damour and V. F. Mukhanov, *k-Inflation*, Phys. Lett. B **458**, 209 (1999) [hep-th/9904075];
T. Chiba, T. Okabe and M. Yamaguchi, *Kinetically Driven Quintessence*, Phys. Rev. D **62**, 023511 (2000) [astro-ph/9912463];
C. Armendariz-Picon, V. F. Mukhanov and P. J. Steinhardt, *A Dynamical Solution to the Problem of a Small Cosmological Constant and Late-time Cosmic Acceleration*, Phys. Rev. Lett. **85**, 4438 (2000) [astro-ph/0004134];
C. Armendariz-Picon, V. F. Mukhanov and P. J. Steinhardt, *Essentials of k-essence*, Phys. Rev. D **63**, 103510 (2001) [astro-ph/0006373];
R. de Putter, E. V. Linder, *Kinetic k-essence and Quintessence*, Astropart. Phys. **28**, 263 (2007) [arXiv:0705.0400 [astro-ph]];
C. Quercellini, M. Bruni and A. Balbi, *Affine equation of state from quintessence and k-essence fields*, Class. Quantum Grav. **24**, 5413 (2007) [arXiv:0706.3667 [astro-ph]];
R. J. Yang, S. N. Zhang and Y. Liu, *Constraints on the generalized tachyon field models from latest observational data*, J. Cosmol. Astropart. Phys. (JCAP) **01**, 017 (2008) [arXiv:0802.2358 [astro-ph]];
L. Á. Gergely and S. Tsujikawa, *Effective field theory of modified gravity with two scalar fields: dark energy and dark matter*, Phys Rev. D **89**, 064059 (2014) [arXiv:1402.0553 [hep-th]].

[4] A. Sen, *Tachyon Matter*, J. High Energy Phys. 02**07**, 065 (2002) [hep-th/0203265];
G. W. Gibbons, *Cosmological Evolution of the Rolling Tachyon*, Phys. Lett. B **537**, 1 (2002) [hep-th/0204008];
T. Padmanabhan, *Accelerated expansion of the universe driven by tachyonic matter*, Phys. Rev. D **66**, 021301 (2002) [hep-th/0204150];
A. Frolov, L. Kofman and A. Starobinsky, *Prospects and Problems of Tachyon Matter Cosmology*, Phys. Lett. B **545**, 8 (2002) [hep-th/0204187];
E. J. Copeland, M. R. Garousi, M. Sami and S. Tsujikawa, *What is needed of a tachyon if it is to be the dark energy?*, Phys. Rev. D **71**, 043003 (2005) [hep-th/0411192];
R. Lazkoz, *Rigidity of cosmic acceleration in a class of k-essence cosmologies*, Int. J. Mod. Phys. D **14**, 635 (2005) [gr-qc/0410019];
V. Gorini, A. Kamenshchik, U. Moschella, V. Pasquier and A. Starobinsky, *Stability properties of some perfect fluid cosmological models*, Phys. Rev. D **72**, 103518 (2005) [astro-ph/0504576];
J. Martin and M. Yamaguchi, *DBI-essence*, Phys. Rev. D **77**, 123508 (2008) [arXiv:0801.3375 [hep-th]];

[5] M. C. Bento, O. Bertolami and A. A. Sen, *Generalized Chaplygin gas and CMBR constraints*, Phys. Rev. D **67**, 063003 (2003) [astro-ph/0210468];
D. Carturan and F. Finelli, *Cosmological Effects of a Class of Fluid Dark Energy Models*, Phys. Rev. D **68**, 103501 (2003) [astro-ph/0211626];
R. Bean and O. Dore, *Are Chaplygin gases serious contenders to the dark energy throne?*, Phys. Rev. D **68**, 023515 (2003) [astro-ph/0301308];
L. M. G. Beca, P. P. Avelino, J. P. M. de Carvalho and C. J. A. P. Martins, *The Role of Baryons in Unified Dark Matter Models*, Phys. Rev. D **67**, 101301 (2003) [astro-ph/0303564];
P. P. Avelino, L. M. G. Beca, J. P. M. de Carvalho and C. J. A. P. Martins, *The ΛCDM Limit of the Generalized Chaplygin Gas Scenario*, J. Cosmol. Astropart. Phys. (JCAP) **09**, 002 (2003) [astro-ph/0307427];
G. M. Kremer, *Cosmological models described by a mixture of van der Waals fluid and dark energy*, Phys. Rev. D **68**, 123507 (2003) [gr-qc/0309111];
M. C. Bento, O. Bertolami and A. A. Sen, *WMAP Constraints on the Generalized Chaplygin Gas Model*, Phys. Lett. B **575**, 172 (2003) [astro-ph/0303538];

L. Amendola, F. Finelli, C. Burigana and D. Carturan, *WMAP and the Generalized Chaplygin Gas*, J. Cosmol. Astropart. (JCAP) **07**, 005 (2003) [astro-ph/0304325];

H. Sandvik, M. Tegmark, M. Zaldarriaga and I. Waga, *The end of unified dark matter?*, Phys. Rev. D **69**, 123524 (2004) [astro-ph/0212114];

P. P. Avelino, L. M. G. Beca, J. P. M. de Carvalho, C. J. A. P. Martins and E. J. Copeland, *The onset of the non-linear regime in unified dark matter models*, Phys. Rev. D **69**, 041301 (2004) [astro-ph/0306493];

A. Dev, D. Jain and J. S. Alcaniz, *Constraints on Chaplygin quartessence from the CLASS gravitational lens statistics and supernova data*, Astron. Astrophys. **417**, 847 (2004) [astro-ph/0311056];

Z.-H. Zhu, *Generalized Chaplygin gas as a unified scenario of dark matter/energy: observational constraints*, Astron. Astrophys. **423**, 421 (2004) [astro-ph/0411039];

C. S. J. Pun, L. Á. Gergely, M.K. Mak, Z. Kovács, G. M. Szabó and T. Harko, *Viscous dissipative Chaplygin gas dominated homogenous and isotropic cosmological models*, Phys. Rev. D **77**, 063528 (2008) [arXiv:0801.2008 [gr-qc]].

[6] J. S. Bagla, H. K. Jassal and T. Padmanabhan, *Cosmology with tachyon field as dark energy*, Phys. Rev. D **67**, 063504 (2003) [astro-ph/0212198].

[7] O. Sergijenko, R. Durrer and B. Novosyadlyj, *Observational constraints on scalar field models of dark energy with barotropic equation of state*, J. Cosmol. Astropart. Phys. (JCAP) **08**, 004 (2011) [arXiv:1102.3168 [astro-ph]];

B. Novosyadlyj, O. Sergijenko, R. Durrer and V. Pelykh, *Constraining the dynamical dark energy parameters: Planck-2013 vs WMAP9*, J. Cosmol. Astropart. Phys. (JCAP) **05**, 030 (2014) [arXiv:1312.6579 [astro-ph]].

[8] V. Gorini, A. Yu. Kamenshchik, U. Moschella and V. Pasquier, *Tachyons, Scalar Fields and Cosmology*, Phys. Rev. D **69**, 123512 (2004) [hep-th/0311111].

[9] J. D. Barrow, G. J. Galloway and F. J. Tipler, *The closed-universe recollapse conjecture*, Mon. Not. R. Astron. Soc. **223**, 835 (1986);

Yu. Shtanov and V. Sahni, *New Cosmological Singularities in Braneworld Models*, Class. Quantum Grav. **19**, L101 (2002) [gr-qc/0204040];

J. D. Barrow, *Sudden Future Singularities*, Class. Quantum Grav. **21**, L79 (2004) [gr-qc/0403084];

J. D. Barrow, *More General Sudden Singularities*, Class. Quantum Grav. **21**, 5619 (2004) [gr-qc/0409062];

M. P. Dabrowski, T. Denkiewicz and M. A. Hendry, *How far is it to a sudden future singularity of pressure?*, Phys. Rev. D **75**, 123524 (2007) [arXiv:0704.1383 [astro-ph]];

A. Yu. Kamenshchik, C. Kiefer and B. Sandhöfer, *Quantum cosmology with big-brake singularity*, Phys. Rev. D **76**, 064032 (2007) [arXiv:0705.1688 [gr-qc]];

L. Fernández-Jambrina and R. Lazkoz, *Singular fate of the universe in modified theories of gravity*, Phys. Lett. B **670**, 254 (2009) [arXiv:0805.2284 [gr-qc]];

J. D. Barrow, A. B. Batista, G. Dito, J. C. Fabris and M. J. S. Houndjo, *Sudden singularities survive massive quantum particle production*, Phys. Rev. D **84**, 123518 (2011) [arXiv:1110.1321 [gr-qc]];

T. Denkiewicz, M.P. Dabrowski, H. Ghodsi and M. A. Hendry, *Cosmological tests of sudden future singularities*, Phys. Rev. D **85**, 083527 (2012) [arXiv:1201.6661 [astro-ph]];

A. Yu. Kamenshchik and S. Manti, *Classical and quantum Big Brake cosmology for scalar field and tachyonic models*, Phys. Rev. D **85**, 123518 (2012) [arXiv:1202.0174 [gr-qc]];

J. D. Barrow and S. Cotsakis, *General Dynamics of Varying-Alpha Universes*, Phys. Rev. D **88**, 067301 (2013) [arXiv:1307.6816 [gr-qc]].

[10] Z. Keresztes, L. Á. Gergely, V. Gorini, U. Moschella and A.Yu. Kamenshchik, *Tachyon cosmology, supernovae data and the Big Brake singularity*, Phys. Rev. D **79**, 083504 (2009) [arXiv:0901.2292 [gr-qc]].

[11] Z. Keresztes, L. Á. Gergely, A. Yu. Kamenshchik, V. Gorini and D. Polarski, *Will the tachyonic Universe survive the Big Brake?*, Phys. Rev. D **82**, 123534 (2010) [arXiv:1009.0776 [gr-qc]].

[12] Z. Keresztes, L. Á. Gergely, A. Yu. Kamenshchik, V. Gorini and D. Polarski, *Soft singularity crossing and transformation of matter properties*, Phys. Rev. D **88**, 023535 (2013) [arXiv:1304.6355 [gr-qc]].

[13] Z. Keresztes, L. Á. Gergely and A. Yu. Kamenshchik, *The paradox of soft singularity crossing and its resolution by distributional cosmological quantities*, Phys. Rev. D **86**, 063522 (2012) [arXiv:1204.1199 [gr-qc]].

[14] N. Suzuki, D. Rubin, C. Lidman et al., *The Hubble Space Telescope Cluster Supernova Survey: V. Improving the Dark Energy Constraints Above $z > 1$ and Building an Early-Type-Hosted Supernova Sample*, Astrophys. J. **746**, 85 (2012) [arXiv:1105.3470 [astro-ph]].

[15] O. Farooq and B. Ratra, *Hubble parameter measurement constraints on the cosmological deceleration-acceleration transition redshift*, Astrophys. J. Lett. **766**, L7 (2013) [arXiv:1301.5243 [astro-ph]].

[16] Y. Chen, C-Q. Geng, S. Cao, Y-M. Huang, Z.-H. Zhu, *Constraints on a ϕCDM model from strong gravitational lensing and updated Hubble parameter measurements*, (2014) [arXiv:1312.1443 [astro-ph]].

[17] A. G. Riess, L. Macri, S. Casertano et al., *A 3% Solution: Determination of the Hubble Constant with the Hubble Space Telescope and Wide Field Camera 3*, Astrophys. J. **730**, 119 (2011); [erratum ibid. **732**, 129 (2011)] [arXiv:1103.2976 [astro-ph]].

[18] P. A. R. Ade, N. Aghanim, C. Armitage-Caplan et al., *Planck 2013 results. XVI. Cosmological parameters*, (2013) [arXiv:1303.5076 [astro-ph]].

[19] T. Delubac, J. E. Bautista, N. G. Busca et al., *Baryon Acoustic Oscillations in the Lyα forest of BOSS DR11 quasars*, (2014) [arXiv:1404.1801 [astro-ph]].

[20] A. Sen, *Rolling Tachyon*, J. High Energy Phys. **04**, 048 (2002) [hep-th/0203211].

[21] V. Sahni, A. Shafieloo, A. A. Starobinsky, *Model independent evidence for dark energy evolution from Baryon Acoustic Oscillations*, Astrophys. J. Lett. **793**, L40 (2014) [arXiv:1406.2209 [astro-ph]].

[22] B. Fields, S. Sarkar, Big-Bang nucleosynthesis (Particle Data Group mini-review), J. Phys. G **33**, 1 (2006) [astro-ph/0601514].

[23] M. R. Garousi, M. Sami and S. Tsujikawa, Phys. Rev. D **70**, 043536 (2004) [hep-th/0402075].

[24] V. Mukhanov, Physical Foundations of Cosmology, Cambridge Univ. Press, Cambridge U.K. (2005).

[25] W. Hu and N. Sugiyama, *Small Scale Cosmological Perturbations: An Analytic Approach*, Astrophys. J. **471**, 542 (1996) [astro-ph/9510117].

[26] A. Challinor and A. Lasenby, *Cosmic microwave background anisotropies in the CDM model: a covariant and gauge-invariant approach*, Astrophys. J. **513**, 1 (2000) [astro-ph/9804301].

[27] A. Lewis, A. Challinor and A. Lasenby, *Efficient Computation of CMB anisotropies in closed FRW models*, Astrophys. J. **538**, 473 (2000) [astro-ph/9911177].

[28] http://camb.info

[29] S. Seager, D. Sasselov and D. Scott, *A New Calculation of the Recombination Epoch*, Astrophys. J. **523**, L1 (1999) [astro-ph/9909275]; W. Y. Wong, A. Moss and D. Scott, *How well do we understand cosmological recombination?*, Mon. Not. Roy. Astron. Soc. **386**, 1023 (2008) [arXiv:0711.1357 [astro-ph]]; http://www.astro.ubc.ca/people/scott/recfast.html

[30] C. Blake, E. Kazin, F. Beutler et al., *The WiggleZ Dark Energy Survey: mapping the distance-redshift relation with baryon acoustic oscillations*, Mon. Not. Roy. Astron. Soc. **418**, 1707 (2011) [arXiv:1108.2635 [astro-ph]].

[31] S. Basilakos, S. Nesseris and L. Perivolaropoulos, *Observational constraints on viable f(R) parametrizations with geometrical and dynamical probes*, Phys. Rev. D **87**, 123529 (2013) [arXiv:1302.6051 [astro-ph]].

[32] L. Anderson, E. Aubourg, S. Bailey et al., *The clustering of galaxies in the SDSS-III Baryon Oscillation Spectroscopic Survey: Baryon Acoustic Oscillations in the Data Release 9 Spectroscopic Galaxy Sample*, Mon. Not. Roy. Astron. Soc. **427**, 3435 (2012) [arXiv:1203.6594 [astro-ph]].

[33] A. L. King, T. M. Davis, K. Denney et al., *High Redshift Standard Candles: Predicted Cosmological Constraints*, Mon. Not. Roy. Astron. Soc. **441**, 3454 (2014) [arXiv:1311.2356 [astro-ph]].

[34] W. Hu and N. Sugiyama, *Toward Understanding CMB Anisotropies and Their Implications*, Phys. Rev. D **51**, 2559 (1995) [astro-ph/9411008].

[35] L. S. Daniel and D. Huterer, *Chasing the phantom: A closer look at Type Ia supernovae and the dark energy equation of state*, Phys. Rev. D **89**, 063510 (2014) [arXiv:1312.1688 [astro-ph]].

[36] S. W. Hawking, *Perturbations of an Expanding Universe*, Astrophys. J. **145**, 544 (1966);
G. F. R. Ellis, *Relativistic Cosmology*, in General Relativity and Cosmology edited by R. K. Sachs, Academic Press, New York (1971);
M. Bruni, P. K. S. Dunsby and G. F. R. Ellis, *Cosmological perturbations and the physical meaning of gauge-invariant variables*, Astrophys. J. **395**, 34 (1992);
R. Maartens, T. Gebbie and G. F. R. Ellis, *Cosmic microwave background anisotropies: Nonlinear dynamics*, Phys. Rev. D **59**, 083506 (1999) [astro-ph/9808163];
T. Gebbie, P. K. S. Dunsby and G. F. R. Ellis, *1+3 Covariant Cosmic Microwave Background anisotropies II: The almost - Friedmann Lemaitre model*, Annals Phys. **282**, 321 (2000) [astro-ph/9904408];
A. Challinor, *Microwave background anisotropies from gravitational waves: the 1+3 covariant approach*, Class. Quantum Grav. **17**, 871 (2000) [astro-ph/9906474];
A. Challinor, *Microwave background polarization in cosmological models*, Phys. Rev. D **62**, 043004 (2000) [astro-ph/9911481];
A. Lewis and A. Challinor, *Evolution of cosmological dark matter perturbations*, Phys. Rev. D **66**, 023531 (2002) [astro-ph/0203507];
A. Lewis, *CMB anisotropies from primordial inhomogeneous magnetic fields*, Phys. Rev. D **70**, 043011 (2004) [astro-ph/0406096].

[37] G. F. R. Ellis, J. Hwang and M. Bruni, *Covariant and gauge-independent perfect-fluid Robertson-Walker perturbations*, Phys. Rev. D **40**, 1819 (1989);
T. Gebbie and G. F. R. Ellis, *1+3 Covariant Cosmic Microwave Background anisotropies I: Algebraic relations for mode and multipole representations*, Annals Phys. **282**, 285 (2000) [astro-ph/9804316].

[38] C.-P. Ma and E. Bertschinger, *Cosmological Perturbation Theory in the Synchronous and Conformal Newtonian Gauges*, Astrophys. J. **455**, 7 (1995) [astro-ph/9506072].